Journal of Unconventional Oil and Gas Resources 8 (2014) 14–24

Contents lists available at ScienceDirect

Journal of Unconventional Oil and Gas Resources

journal homepage: www.elsevier.com/locate/juogr

Adsorption of methane and carbon dioxide on gas shale and pure mineral samples

Robert Heller *, Mark Zoback

Department of Geophysics, Stanford University, Stanford, CA, United States

ARTICLE INFO

Article history:
Received 9 August 2013
Revised 27 June 2014
Accepted 27 June 2014
Available online 27 July 2014

Keywords:
Shale
Adsorption
Carbon dioxide
Clay
Illite
Swelling

ABSTRACT

We have measured methane and carbon dioxide adsorption isotherms at 40 °C on gas shale samples from the Barnett, Eagle Ford, Marcellus and Montney reservoirs. Carbon dioxide isotherms were included to assess its potential for preferential adsorption, with implications for its use as a fracturing fluid and/or storage in depleted shale reservoirs. To better understand how the individual mineral constituents that comprise shales contribute to adsorption, measurements were made on samples of pure carbon, illite and kaolinite as well. We were able to successfully fit all adsorption data for both gases in accordance with a Langmuir isotherm model. Our results show carbon dioxide to have approximately 2–3 times the adsorptive capacity of methane in both the pure mineral constituents and actual shale samples. In addition to obvious microstructural and compositional differences between real rocks and pure minerals, we hypothesize that water adsorption plays an important role in regulating surface area availability for other molecules to adsorb. The resultant volumetric swelling strain was also measured as a function of pressure/adsorption. We observe both clay and pure carbon to swell an amount that is approximately linearly proportional to the amount of adsorption.

Introduction

Gas shales are complex rocks, characterized by heterogeneity in composition and structure at all scales. Similarly, the production of natural gas from shales is controlled by phenomena acting at many different scales, as has been reviewed by several authors (Bustin et al., 2008; Loucks et al., 2009; Wang and Reed, 2009; Sondergeld et al., 2010). One potentially significant property impacting production from these reservoirs is the adsorption of methane, which is controlled by the composition and microstructure of the rock. By storing gas in a dense, liquid-like adsorbed phase, the overall storage capacity of the rock is enhanced relative to if there were a free phase alone. Moreover, the release of this adsorbed phase is pressure dependent. As a reservoir is depleted, the adsorbed phase is freed, providing not just additional gas for production but helping to sustain pressure (and perhaps open pore throats for fluid flow) as well. While adsorption allows for larger quantities of gas to be in place and possibly produced, factors such as desorption pressure, kinetics, and alteration of effective stresses makes it difficult to know if desorbed gas will contribute significantly to production.

In an effort to better understand the role of adsorption on production from gas shales, numerous authors have made valuable contributions to the literature through laboratory studies over the last 25 years. Schettler et al. (1991) performed experiments on pure clay, carbon and quartz minerals in addition to Devonian shales in an attempt to shed light on some of the factors affecting adsorption. They noted the significant adsorptive capacity of all of these minerals when measured individually. In addition, they found some cases in which the shape of the shale adsorption isotherm was best explained by adsorption on carbon (a proxy for kerogen), while others were better explained by illite adsorption. Similarly, Lu et al. (1995) measured the adsorptive capacity of several Devonian shale samples and pure illite. They concluded that while total organic content (TOC) played a first order role in the adsorptive capacity of their samples, illite was also responsible for significant gas storage, particularly in samples with little TOC.

More recent efforts have reached quite similar conclusions to previous studies. Ross and Bustin (2009) performed a laboratory investigation of the impact of composition and pore structure on total storage capacity in gas shales. In addition to carbon, they measured significant microporosity in clay minerals, particularly illite and montmorillonite. Chalmers and Bustin (2008) studied the impact of kerogen type and other geochemical properties on adsorption. They found that types I, II and II kerogen are all capable

* Corresponding author.
E-mail address: robert.heller@bp.com (R. Heller).

http://dx.doi.org/10.1016/j.juogr.2014.06.001
2213-3976/

of equally significant amounts of adsorption, but for differing reasons. Furthermore, they highlighted complexities associated with water content competing with adsorption sites in some cases (but not others) depending on geochemical composition and pore structure.

In addition to methane, there have been several studies highlighting the adsorptive capacity of carbon dioxide in gas shales. Nuttall et al. (2005) measured CH_4 and CO_2 adsorption on Devonian black shales in order to assess the potential for enhanced recovery or sequestration. They found CO_2 to have a adsorption capacity approximately 5 times greater than that of CH_4. Similarly, Kang et al. (2010) studied the adsorption of both gases on two samples from the Barnett shale, finding CO_2 to adsorb 5–10 times more than CH_4.

While ubiquitous in the coalbed methane literature, there is very limited data available to predict the accompanying volumetric strain caused by desorption during production or adsorption during gas injection. Lin et al. (2007) measured volumetric swelling strain resulting from adsorption of N_2, CH_4 and CO_2 in coal samples. They found roughly a linear relationship between swelling strain and adsorption. Similarly, Hol et al. (2011) studied the link between adsorption, swelling and stress in coal. Their results also show a linear relationship between adsorption and swelling. Moreover, they demonstrate the quantity of adsorption/desorption at a given pressure to be significantly influenced by the magnitude of external stress on the rock. Several authors have suggested the potential importance of adsorption-induced deformation in the context of gas shales (Cui et al., 2009; Ross and Bustin, 2007), however, no efforts have directly addressed the topic to date.

In this study, we extend these previous works and investigate the adsorption of CH_4 and CO_2 on various shale and pure mineral samples in the laboratory. Samples from four different formations were studied, as well as pure carbon, illite and kaolinite. Using the methods described below, we measured the adsorption of CH_4 and CO_2 on both shale samples and pure minerals. In a triaxial apparatus, the resultant volumetric swelling strain associated with adsorption is measured. Our overall objective is to further the effort toward understanding adsorption in gas shales. In addition, the experimental results are analyzed and discussed in the context of production from gas shales.

Sample description

Experiments were first carried out on pure carbon and clay materials. Activated carbon (Filtrasorb 400, 12 × 40 mesh) was purchased from Calgon Carbon to be representative of mature kerogen. Kaolinite and illite samples were obtained from the Clay Mineral Society and sold to us as pure clay samples. Both CH_4 and CO_2 adsorption isotherms were measured for each of these materials. Following these experiments, the adsorption of CH_4 and CO_2 was measured on gas shale samples from the Barnett, Marcellus, Eagle Ford and Montney reservoirs. To the degree possible, samples of representative mineralogical composition were selected from each of these shales. The Barnett sample was highest in TOC (>5%) and had a relatively high clay content (37.4%) as well. The Montney sample and Eagle Ford samples had a similar amount of TOC (2.0% and 1.8%, respectively), but the Montney sample had much more clay and quartz whereas the Eagle Ford was mostly carbonate (>70%). The Marcellus sample was lowest in TOC (1.2%) and had the highest amount of clay (~50%). A complete description of the mineralogy of these samples is provided in Table 1.

In addition to mineralogy, Rock Eval Pyrolisis data was gathered on three of the four samples. This data is also presented in tabulated format in Table 1. Rock Eval Pyrolisis involves heating a small amount of ground up sample at a constant rate (5 °C/min, in this case), and measuring the hydrocarbons produced from the sample as a function of temperature. The S1 and S2 peaks quantify the amount of hydrocarbon thermally extracted at approximately 300 °C and 550 °C, respectively. S1 essentially indicates that amount of free hydrocarbons (gas or oil) present in the sample, while S2 is a better indication of hydrocarbon generation potential upon further heating and burial. S3 quantifies the amount of CO_2 relieved from the organic matter during pyrolisis of kerogen, and is indicative of the amount of oxygen in the kerogen. The Tmax temperature indicates that temperature at which the S2 peak reaches a maximum, which serves as an indication of the maturation stage of the organic matter. The hydrogen index (HI) and oxygen index (OI) can be calculated from this data, and are typically used to characterize the origin of the organic matter. All of this information can be combined to delineate whether the sample lies within the immature, oil, condensate or dry gas window (Peters and Moldowan, 1993). Of the three samples tested, only one lies conclusively within the dry gas window (Eagle Ford 127). The Barnett 31 and Marcellus samples lie within the condensate and late-oil windows, respectively.

Table 1
Sample mineralogy and Rock Eval Pyrolisis data. Pyrolisis data indicates that the Eagle Ford 127 sample to lies within the dry gas window, while the Barnett and Marcellus samples are less mature and slightly more oil-prone.

	Barnett 31	Eagle Ford 127	Marcellus	Montney
Depth (ft)	8640.8	12,771.35	6300	7614.52
Depth (m)	2633.7	3893.70	1920.73	2321.50
Initial Mass (g)	41.32	46.46	34.42	38.33
Mass After Drying (g)	41.19	46.35	34.34	38.22
Water by Mass%	0.31	0.24	0.22	0.28
TOC (%)	5.3	1.8	1.2	2.0
Quartz (%)	51.3	7.0	38.0	42.3
Plagioclase/Feldspar (%)	4.0	4.0	6.0	11.9
Calcite (%)	0.0	80.0	1.0	8.1
Dolomite (%)	0.4	1.0	1.0	9.9
Pyrite (%)	1.7	1.0	1.0	3.5
Apatite (%)	0.0	2.0	1.0	0.0
Total Clay (%)	37.4	5.0	52.0	24.1
S1 (mg HC/g rock)	4.4	2.88	2.06	N/A
S2 (mg HC/g rock)	6.1	1.36	5.15	N/A
S3 (mg HC/g rock)	0.3	0.54	0.31	N/A
Tmax (°C)	452	466	369	N/A
HI (mg HC/g TOC)	115	75	439	N/A
OI (mg CO_2/g TOC)	6	30	26	N/A

Methodology & background

Adsorption measurements

The adsorptive potential for a material is quantified by measuring the surface uptake of an adsorbate over a series of pressures at constant temperature, defining what is called an adsorption isotherm. In addition to describing adsorptive capacity, the magnitude and shape of the isotherm gives insight into pore structure and surface properties of the material. In general, the more surface area and the stronger the adsorbate–adsorbent interaction energy, the greater the amount of adsorption. However, pore size distribution also plays an important role. As pores become smaller and smaller, molecules residing within such pores become increasingly more impacted by the enclosing surfaces on all sides. In other words, the interaction energy from multiple surfaces coalesce, resulting in an overall increase in attraction relative to a free surface. Thus, materials with a large micropore volume are generally very adsorptive. When performing calculations or making inferences about pore structure and surface area from adsorption

isotherms, it is important to distinguish between these two distinctly different mechanisms (surface adsorption versus micropore volume filling). However, it is worth keeping in mind that the net effect is exactly the same: molecules are stored in a denser phase relative to the free gas phase.

The experiments reported here were performed on crushed samples with a particle size between 50 and 150 microns. While it is possible to perform adsorption experiments on intact core samples, the time required to reach equilibrium would be prohibitively long due to the extremely low permeability of shales (Heller et al., 2014). Therefore, measuring adsorption on crushed samples is preferred. Approximately 40 g of sample was used for each experiment. After crushing, samples were placed in a vacuum oven at 40 °C until constant mass was achieved. The temperature was chosen so as to be above the boiling point of water in near vacuum conditions, but not so high as to remove clay-bound water and alter the clay properties. Once dried, the sample was loaded into the sample cell and again placed under vacuum to remove water and gas that may have contaminated the sample during loading.

Procedures for measuring adsorption are well established, and can generally fall into the category of either mass-based or volumetric-based methods. Mass-based methods employ the use of a microbalance to directly measure the change in sample mass associated with adsorption, and are very commonly used in material science. The advantage of mass-based methods is a very high degree of accuracy, with the trade-off being the need to use very small sample sizes. Given the heterogeneity of rocks, the oil and gas industry has generally favored the volumetric method (as used in this study), which allows us to use much larger sample volumes.

The volumetric method is based on Boyle's law, and is very similar to porosity measurements using pycnometry. The system consists of two chambers (termed the reference cell and sample cell) separated by a valve, all placed within a controlled temperature bath, as shown in Fig. 1. The reference cell volume, V_R, is a known value, calibrated against the volume of carefully machined aluminum plugs. The crushed particles are loaded into the sample cell and the void volume, V_S, (comprised of space within lines, between particles and particle porosity) is determined via multiple expansions of helium from the reference cell volume, V_R. Each expansion involves first pressurizing the reference cell, and quantifying the number of molecules loaded into the cell as follows:

$$n_{\text{total}} = \frac{P_1 V_R}{Z_1 R T_1} \tag{1}$$

where V_R is the reference cell volume, P_1 the pressure, Z_1 the compressibility factor, R the universal gas constant and T_1 is the temperature which was that of the oil bath, set to 40 °C. The valve separating the reference cell and sample cell is then opened, allowing the gas to expand into the void volume of the sample cell. By selecting what is assumed to be a non-adsorbing gas for this process (helium), the subsequent pressure drop once the valve is opened is due to void volume filling. Therefore the number of free molecules in the system is unchanged, and the void volume of the sample cell can be calculated as follows:

$$V_S = \frac{n_{\text{total}} Z_2 R T_2}{P_2} - V_R \tag{2}$$

where P_2, Z_2 and T_2 are the pressure, compressibility factor and temperature at equilibrium after the valve is opened. All compressibility factors (Z) were determined using NIST's REFPROP program (NIST, 2007). This program provides tables of the most accurate equations of state available for all gases considered in this study, allowing the user to lookup compressibility factors at any pressure and temperature for each gas.

Some authors have suggested a pressure dependent void volume of the reference cell, owing to helium achieving a higher capacity to access finer and finer pores at higher pressures (Ross and Bustin, 2007). Given these observations, we measured the reference cell volume over a range of equilibrium pressures. However, we observed no variation in void volume with pressure in our tests. An example of a typical void volume versus pressure measurement is shown in Fig. 2. This particular example is for the Eagle Ford shale sample.

Following void volume measurement with helium, the system was again vacuumed to remove any residual helium that may have been trapped within the lines or sample particles. With the void volume of the reference cell determined, one can then perform expansions of an adsorbing gas into the sample in the same manner already described. However, during the expansion of an adsorbing gas from the reference cell to the sample, the pressure will decrease due to both void volume filling as well as adsorption (adsorbed molecules are bound, and thus have no kinetic energy and do not contribute to the gas phase pressure). Thus, the amount of adsorption is the calculated as follows:

$$n_{\text{ads}}^{\text{excess}} = n_{\text{total}} - n_{\text{free}} \tag{3}$$

where n_{total} is the number of moles originally in the reference cell (the number of moles expected to be in the system if no adsorption occurred), and n_{free} is the number of molecules in the free phase at equilibrium, calculated as:

$$n_{\text{free}} = \frac{P_2 (V_R + V_S)}{R T_2 Z_2} \tag{4}$$

where V_R and V_S are the reference and sample cell volumes, respectively. Following a measurement at a single pressure, the valve

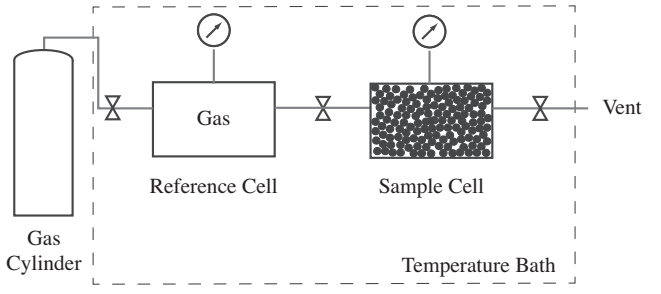

Fig. 1. Schematic of system used for adsorption measurements. Both reference and sample cells are placed inside of a temperature controlled oil bath for stability, which was set to 40 °C in all experiments. The volumes of both cells are adjustable using aluminum spacers to accommodate varying sample sizes without sacrificing measurement stability.

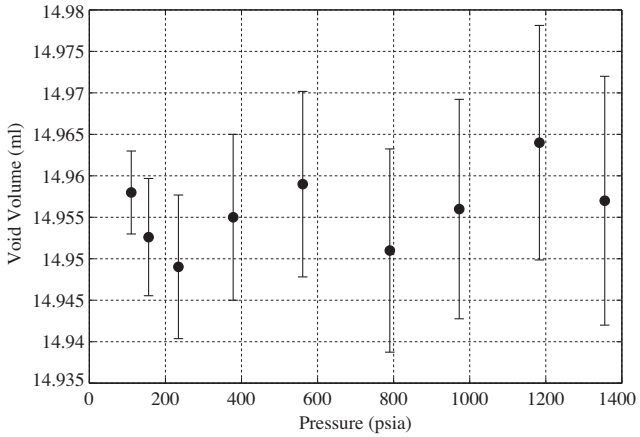

Fig. 2. Void volume versus pressure for the Eagle Ford sample. Note that no dependency of void volume on pressure was observed. Void volume measurement scattered about a mean of 14.956 ml, with as standard deviation of 0.0045 ml.

separating the two chambers is closed, the reference cell charged to a higher pressure and the process repeated until a full isotherm has been characterized.

Adsorption data analysis

The procedure outlined above is for calculating what is termed excess adsorption (or sometimes Gibbs adsorption), referring to the amount adsorbed in excess of that which would be present if the adsorbed-phase volume were filled with bulk gas. In other words, as adsorption occurs, the porosity occupied by the adsorbed phase that is no longer available to free gas must be corrected for. Making this correction is called calculating the absolute, or total, amount of adsorption. Failing to make this correction will result in an underprediction of the adsorbed quantity.

Estimating absolute adsorption from excess adsorption data is a major challenge, requiring knowledge of either the density or volume of the adsorbed phase. There have been very few efforts at directly measuring the specific volume of gas molecules in the adsorbed state. There are three common approaches for approximating this parameter. The first is to use the van der Waals constant b for the density (Dubinin, 1960). Equally common to this approach is to assume the adsorbate density to be that of the liquefied gas just below its boiling point (Tsai et al., 1985). Finally, one might assume the density to be equal to that of the solidified gas. Perhaps complicating matters, arguments have been made for employing a combination of two or more of these assumptions depending on where along the adsorption isotherm the measurement is being made (Menon, 1968).

In this work, we have elected to use the van Der Waals constant b for the adsorbed phase density, as first suggested by Dubinin (1960). After making this assumption, the absolute adsorption can be estimated as follows:

$$n_{\text{ads}}^{\text{absolute}} = \frac{n_{\text{ads}}^{\text{excess}}}{1 - \frac{\rho_{\text{gas}}}{\rho_{\text{ads}}}} \tag{5}$$

where ρ_{gas} is the density of the gas phase and ρ_{ads} is the density of the adsorbed phase.

Once measurements have been complete and the appropriate corrections made, the data can be fit to one of several isotherm models. The most common model used to describe an adsorption isotherm was developed by Langmuir, 1916. The Langmuir isotherm describes a progressively increasing surface occupancy as a function of pressure up until the entire surface area is coated with a single layer of molecules and no further adsorption can occur. The entire isotherm can be fit with a two-parameter equation:

$$V_P = \frac{V_L P}{P_L + P} \tag{6}$$

where V_P is the volume of adsorption at pressure P, V_L is the Langmuir volume, representative of total adsorption at infinite pressure, and P_L is the Langmuir pressure, which is the pressure at which half the Langmuir volume is adsorbed (Langmuir, 1916). Regardless of whether the assumptions of the model are true, the Langmuir-shaped curve is so prolific and the model so simple to apply that it is often selected in fitting experimental data as a matter of practicality. The shapes of all adsorption isotherms presented in this paper are, in fact, well-fit by Langmuir isotherms.

Swelling

As mentioned above, there have been no laboratory studies to date quantifying the volumetric swelling strain associated with adsorption in gas shales. Such experiments are more challenging in the context of shales for several reasons. First, measuring the swelling response to adsorption needs to be performed on intact core plugs, requiring a significant amount of time. Second, given that the amount of adsorption measured on gas shales is approximately an order of magnitude less than what is observed in coal, one can expect at least an order of magnitude less volumetric swelling strain. Finally, shales are an order of magnitude stiffer at the bulk scale when compared to coals, further reducing the amount of swelling strain that one might expect to observe with intact core plugs, thus making it very challenging to measure.

We measured volumetric swelling strain resulting from adsorption in a separate series of experiments performed in a triaxial compression apparatus. Samples used in the swelling experiments included carbon, illite and kaolinite. We elected to perform these measurements on pure mineral particles as opposed to crushed or intact shale samples for two reasons. First, it allowed us the advantage of overcoming the challenges associated with long equilibration times and measuring very small strains, as discussed above. Second, measuring swelling of the individual mineralogical constituents is a simpler way of answering the first order question of whether or not swelling could be important in gas shales.

Measurements were made on the same set of clay and carbon samples, ground to the same particle size and dried for the same period of time under the same conditions. A combination of two jackets were used to isolate the sample and pore fluid from the confining fluid, which included both copper as wells as a Viton jacket. The thin copper jacket was chosen for the inside in order to help prevent the pore fluid from exiting the sample by diffusion. In addition, the copper provided a rigid cylinder within which to place the crushed material and form the synthetic sample. A Viton jacket was chosen on the outside because of its compatibility with our confining oil, as well as the integrity of the seal it formed against the stainless steel coreholders.

The samples were cast inside of a 0.002 inch thick copper jacket that was cut from a sheet and soldered at the seam to form a cylinder that was 1.0 inch in diameter and 2.0 inches in length. The cylinder was first slid over a stainless steel coreholder. A 40 micron aperture circular screen was then cut and placed inside of the cylinder to prevent particles from entering the system plumbing. The copper was then filled with small aliquots of material and tamped until completion, and a second screen was placed on top of the sample. Heat shrinkable Viton tubing was then slid over the outside of the copper, and the top coreholder was placed on the sample. The tubing was then shrunk around the sample, and pre-positioned hose clamps were then tightened around the Viton jacket. A pair of LVDT transducers (1 micron resolution) were attached to the top and bottom coreholders to measure the change in distance between the coreholders. The LVDT coil assembly is fixed within the top coreholder. The LVDT core is attached to a rod with threads at the bottom, fixing it to the bottom coreholder. Finally, sample deformation in the lateral direction was measured by a pair of spring-mounted strain-gauge transducers (0.6 micron resolution; only one is drawn in Fig. 3 for simplification) clamped to the outside of the Viton jacket. The transducers were attached 90 degrees apart from each other to measure the lateral deformation in two directions. All data was recorded digitally on a personal computer equipped with a custom data acquisition system. See Fig. 3 for a schematic of the sample/jacket/coreholder configuration.

In order to form a compact sample from crushed material that behaved as elastically as possible, all samples were stressed to a confining pressure of 30 MPa, which is approximately twice as high the maximum confining pressure the sample would experience during the experiment. The confining pressure was then cycled back and forth between 1 and 30 MPa while the strain was monitored to check for elasticity, which was typically achieved

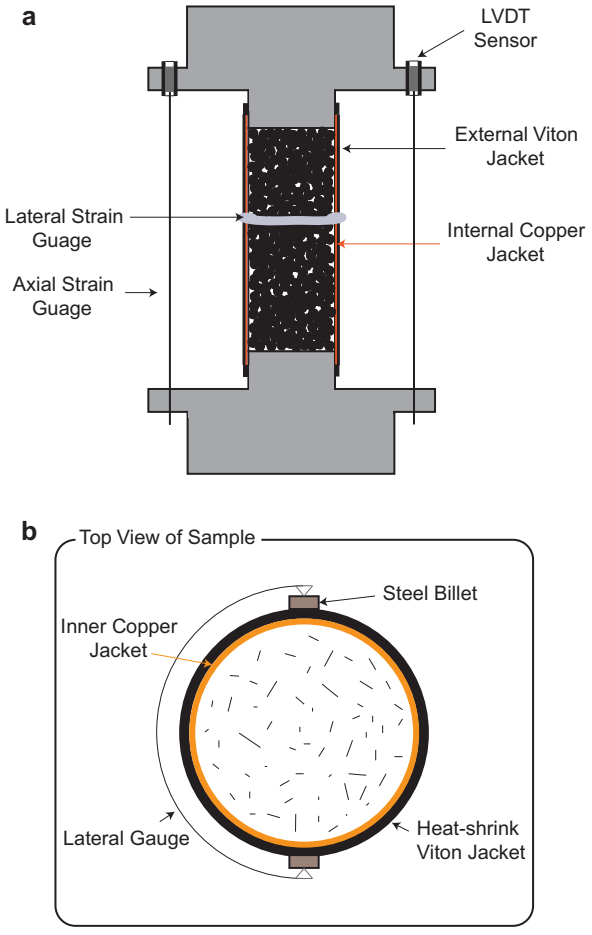

Fig. 3. Schematic of sample setup for swelling experiments. A side view of the entire core holder and sample assembly is shown in (a). A top view of just the jacket and lateral strain gauge configuration is illustrated in (b) (only one of the two lateral gauges is shown for simplicity). The sample was loaded inside of a soldered copper sleeve, encased in heat-shrink Viton tubing to isolate the sample from the confining fluid. Core holders are shown on either end, with axial and lateral strain gauges affixed to the setup as well.

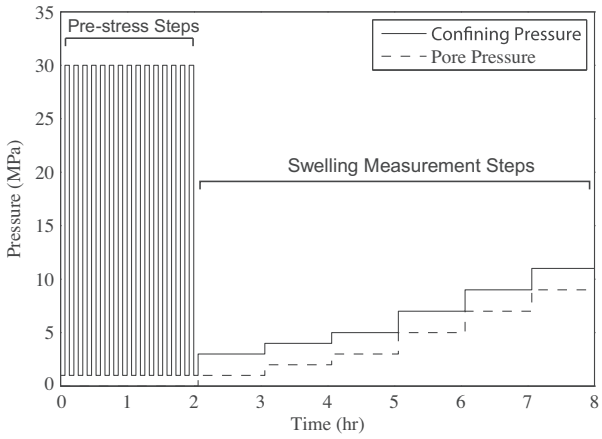

Fig. 4. A typical sequence of confining and pore pressure steps for a single experiment. In order to form a compact sample from crushed material that behaved as elastically as possible, the confining pressure was cycled back and forth between 1 and 30 MPa while the strain was monitored to check for elasticity. Following this sequence, swelling is measured as a series of escalating pore pressures while maintaining a constant effective stress on the sample.

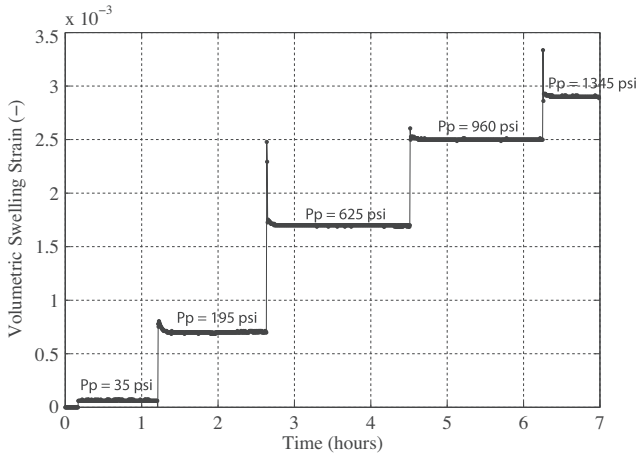

Fig. 5. Volumetric strain signal versus time during an activated carbon swelling experiment with methane as the test gas. Positive strain indicates swelling in this convention.

after about 15 cycles over a two hour period. A typical sequence of confining and pore pressure steps for a single experiment is shown in Fig. 4.

Following sample preparation, the sample was exposed to a series of escalating pore pressures, maintaining a constant differential between the pore pressure and confining pressure of 2 MPa at each step (constant effective stress). Any swelling observed at each step was recorded by the axial and lateral strain gauges attached to the sample setup. An obvious source of error lies in the fact that the measured lateral displacement also includes deformation of the Viton jacket. However, because the effective stress acting on the sample was kept constant, jacket deformation was relatively invariant from one pore pressure step to the next, thus impacting our measurements insignificantly. An example of a typical volumetric strain response measured during an experiment is shown in Fig. 5.

While we attempted to measure swelling at the same pore pressures at which adsorption was measured, a perfect match was not achieved. However, all adsorption data was fit to an isotherm model, allowing for prediction of the adsorbed amount at any point along the curve. This allowed us to compare swelling as a function of adsorbed volume, as opposed to just pore pressure. However, we acknowledge that performing the swelling and adsorption experiments separately could be a source of uncertainty in the results. An additional source of error is that swelling was measured at room temperature (approximately 25 °C) whereas adsorption was measured at 40 °C. Thus, we are likely to be slightly over predicting the swelling response from adsorption. Despite these potential sources of error, we believe the data to be valuable toward developing a phenomenological understanding of the linkage between swelling and adsorption in minerals that comprise shales.

Results

Methane and carbon dioxide adsorption isotherms were measured on samples from the four shale reservoirs described above. All data was successfully fit to Langmuir adsorption isotherms. Fitted adsorption parameters are shown in Table 2, and plots of absolute adsorption are shown in Fig. 6. For all samples, CO_2 exhibited a greater capacity for adsorption relative to CH_4 (about 2 times greater in the Barnett and Marcellus samples, and 3 times greater in the Montney and Eagle Ford samples). Both CH_4 and CO_2 adsorption capacities varied greatly between samples as well, with the Barnett and Montney samples adsorbing considerably more than

Table 2
Langmuir isotherm parameters fit to experimental data. The Barnett sample, which had the highest amount of TOC and a high clay fraction, adsorbed the most out of the gas shale samples. The Montney sample exhibited a fairly high capacity for adsorption despite being comprised of a relatively modest amount of TOC and clay. The Marcellus sample had the lowest TOC content but very high clay content, and adsorbed slightly more than the Eagle Ford. The Eagle Ford sample, which had very little clay and was dominated by carbonate, adsorbed the least.

	Barnett 31	Eagle Ford 127	Marcellus	Montney	Illite	Kaolinite	Carbon
TOC (%)	5.3	1.8	1.2	2.0	0	0	100
Clay (%)	37.4	4.9	51.4	23.7	100	100	0
Methane							
PL (psia)	580.5	694.7	556.2	1283.0	599.6	701.8	452.4
VL (scf/ton)	74.4	12.7	28.3	54.3	133.7	31.7	5,369.6
Carbon dioxide							
PL (psia)	475.1	409.6	263.2	456.0	118.8	358.8	676.2
VL (scf/ton)	147.4	33.1	63.7	153.0	161.2	114.4	26,001.9

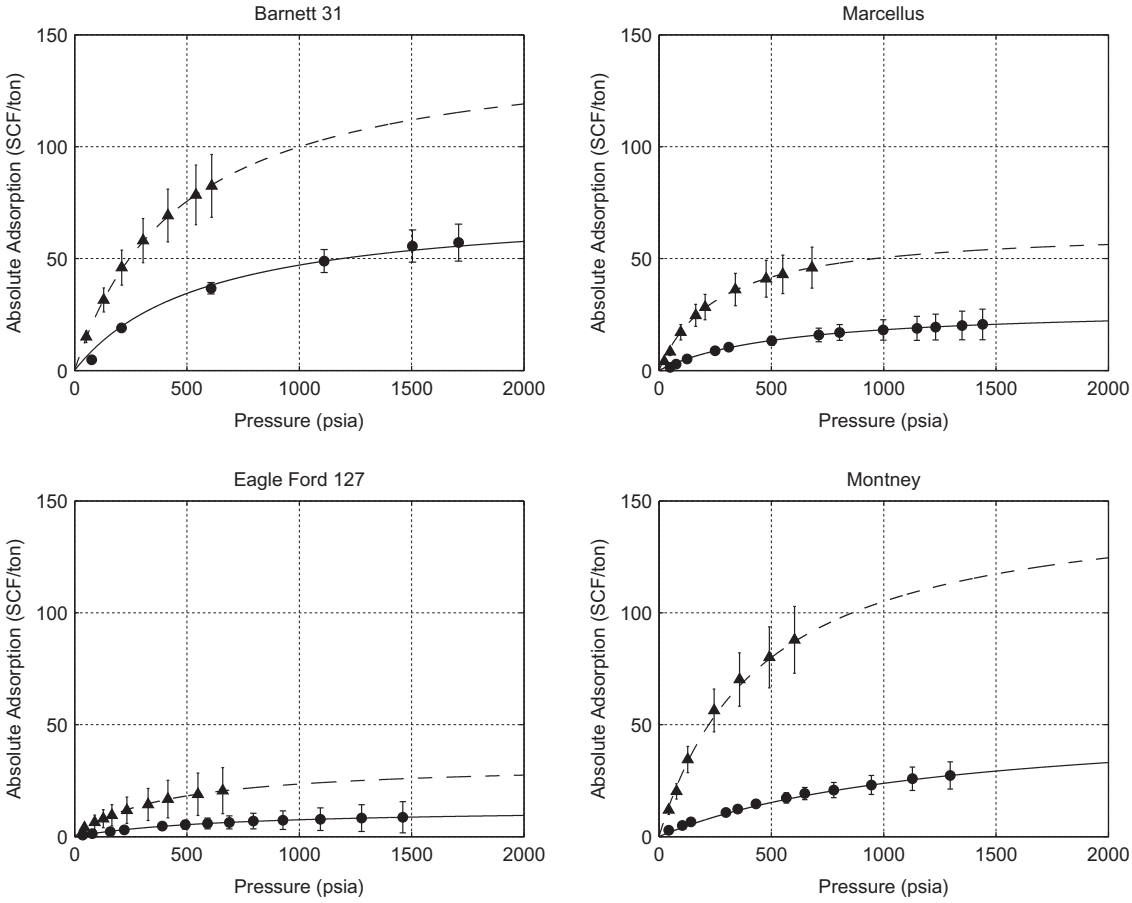

Fig. 6. Methane and carbon dioxide adsorption isotherms on samples from the Barnett, Marcellus, Eagle Ford and Montney shale reservoirs. Points indicate pressures where data was collected, and lines indicate modeled isotherms fit using parameters shown in Table 2. All axes are scaled the same for ease of comparison between samples. For all samples, CO_2 exhibited a greater capacity for adsorption relative to CH_4 (CO_2 about 2× greater in the Barnett and Marcellus, and 3× greater in the Montney and Eagle Ford samples). The Barnett sample adsorbed the most, followed by the Montney, Marcellus and finally the Eagle Ford sample.

the Marcellus and Eagle Ford samples (about 2–6 times more CH_4 and CO_2 adsorption, respectively). A look at the mineralogical differences between these samples indicates that composition was likely a major controlling factor of these differences, but not the only one. The Barnett sample had the highest amount of TOC (5.3%) and also the largest adsorption capacity. Perhaps the most surprising sample was the Montney, which had a modest amount of TOC (2%) and clay (23.7%), but demonstrated a fairly high capacity for adsorption. The Eagle Ford sample was the least adsorptive of all samples, even though it had slightly more TOC than the Marcellus (1.8% vs. 1.2%). If the clay fraction contributes to total adsorption capacity, the difference might be explained by the Marcellus sample having a high clay fraction of 41.3% while the Eagle Ford was mostly carbonate and had just 4.9% clay. However, clay adsorption is just one possible explanation for the observed differences in adsorption capacity. Differences in the maturity of the organic matter and microstructure of the rock may also play a significant role. In general, the greater the maturity of the organic matter the greater the surface area, and thus the greater the adsorptive capacity. The Eagle Ford sample was the most thermally mature but the least adsorptive, perhaps further supporting the hypothesis that other minerals (such as clays) play an important role in adsorption.

Methane and carbon dioxide adsorption isotherms were measured for samples of illite, kaolinite and carbon as well. Again, we were able to successfully fit all data using the Langmuir model.

Fitted adsorption parameters are shown in Table 2, and plots of absolute adsorption are shown in Fig. 7. Similar to the shale adsorption isotherms, CO_2 demonstrated a greater capacity for adsorption relative to CH_4 (at 1000 psi, about 1.5 times greater in illite, 4 times greater in kaolinite, and 3 times greater in carbon). The magnitude of both CH_4 and CO_2 adsorption in all cases is quite significant and beyond what we would expect given the magnitude of adsorption we have measured in our shale samples. To illustrate this point, we calculated hypothetical CH_4 Langmuir volumes for each shale sample, assuming adsorption in shales to be equal to the sum of adsorption by the individual minerals which comprise it. For simplicity, we will also assume all clay to be illite (a close look at the clay XRD data show the clay fraction to be dominated by illite) and that no other minerals present within the samples are capable of adsorption. With these assumptions, one would calculate Langmuir volumes for the Barnett, Eagle Ford, Marcellus and Montney shale samples to be about 4.5 times, 8 times, 4.6 times and 1.9 times what was actually measured, respectively (see Table 3 for details of calculation). Similar results have been found by other authors (Schettler et al., 1991; Lu et al., 1995). These results are considered further in the discussion section.

In addition to adsorption, the volumetric swelling strain associated with the adsorption of CH_4 and CO_2 was measured for the pure mineral samples. The volumetric swelling strain is plotted as a function of the amount of adsorption on a linear scale in Fig. 8a, and on a log–log scale in Fig. 8b. On a linear scale, carbon data must be plotted separately as the amount of adsorption and swelling far exceeds that of illite and kaolinite. On a log–log scale, all data is able to fit on the same graph, and the relative magnitude of adsorption and swelling by the carbon sample is more easily compared to the clay.

The magnitude of the swelling strain measured varied from $\sim 5 \times 10^{-5}$ to $\sim 5 \times 10^{-3}$, or approximately two orders of magnitude. The amount of adsorption causing this swelling strain, varied from about 10^{-1} to 10^{-4}, or nearly 3 orders of magnitude. Viewing the data plotted on a linear scale, we observe both clay and carbon to swell in amount that is roughly linearly proportional to the amount of adsorption. In addition, we observe a similar amount of swelling for a given amount of adsorption on the same sample regardless of whether CH_4 or CO_2 is the adsorbing gas. However, for a given amount of adsorption, the magnitude of swelling observed for each sample was quite different. We attributed this to the difference in the stiffness between samples. While the elastic moduli were not measured, we assume differences in bulk sample stiffness to correlate roughly with the differences in mineral elastic moduli, which are tabulated in Table 3. This data supports the notion that for a given amount of adsorption, the stiffer the mineral, the less the amount of swelling strain.

Discussion

Adsorption

The methane adsorption isotherm we measured on our Barnett shale sample is very similar in both shape and magnitude to those found in the literature. Kang et al. (2010) measured methane adsorption on two Barnett shales at CH_4 pressures in the range of 1000–3000 psi. They measured an adsorption capacity of approximately 40–50 scf/ton at 1000 psi. Montgomery et al. (2005) presented Barnett methane adsorption capacities from 40 to 75 scf/ton at the same pressure. Our measurement of ~50 SCF/ton at

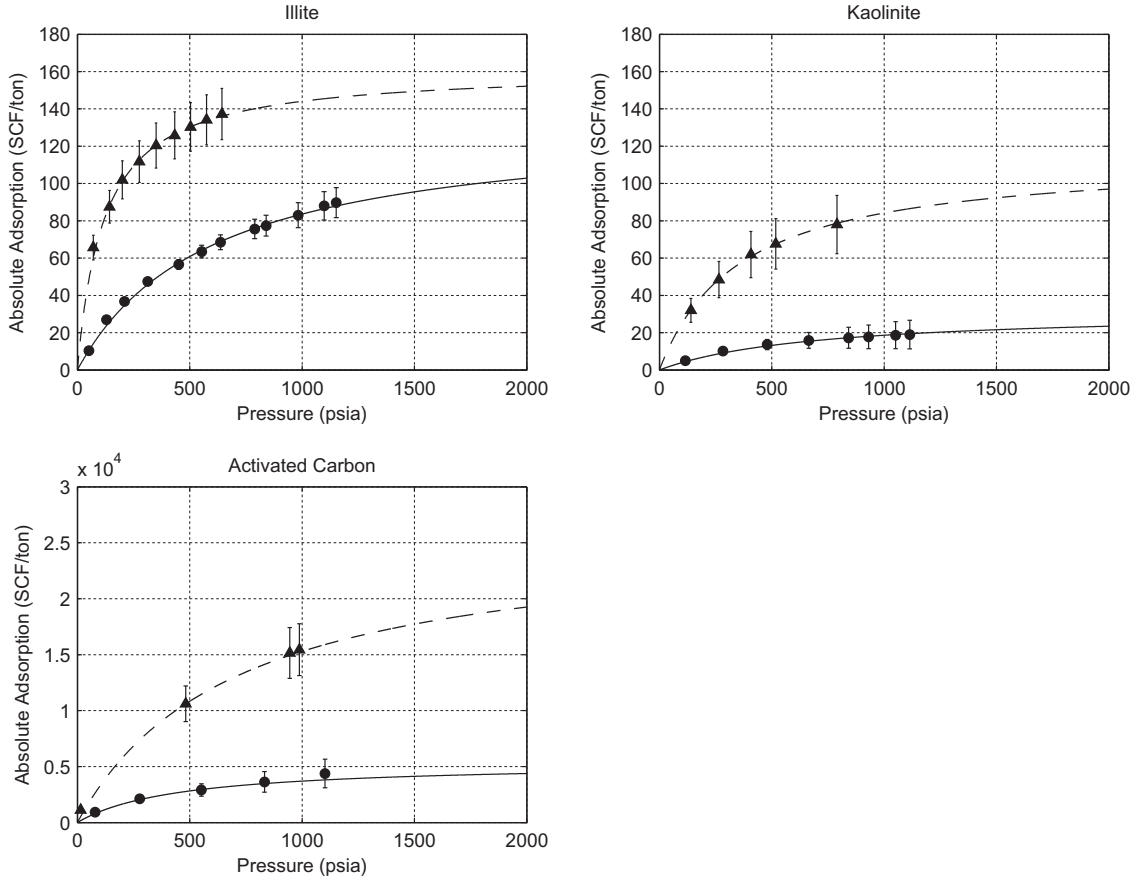

Fig. 7. Methane and carbon dioxide adsorption on samples of pure illite, kaolinite and activated carbon. Note that in the case of activated carbon, the scale is multiplied by a factor of 10,000.

Table 3
Hypothetical CH_4 Langmuir volume calculations for shale samples studied in this work. The results demonstrate that the magnitude of adsorption is drastically over-predicted if one assumes adsorption in shales to be equal to the sum of the adsorption by its mineralogical constituents. The calculated Langmuir volumes are 4.5 times, 8 times, 4.6 times and 1.9 times the measured Langmuir volumes in the Barnett, Eagle Ford, Marcellus and Montney samples, respectively.

	Adsorption from carbon					+	Adsorption from Clay					=	Total adsorption	
	TOC (%)		VL (scf/ton)		Vads (scf/ton)		Clay (%)		VL (scf/ton)		Vads (scf/ton)		Calculated (scf/ton)	Actual (scf/ton)
Barnett 31	5.3	×	5369.6	=	284.3		37.4	×	133.7	=	50.0		334.3	74.4
Eagle Ford 127	1.8	×	5369.6	=	95.5		4.9	×	133.7	=	6.6		102.0	12.7
Marcellus	1.2	×	5369.6	=	62.1		51.4	×	133.7	=	68.7		130.8	28.3
Montney	2.0	×	5369.6	=	107.4		23.7	×	133.7	=	31.7		139.1	73.3

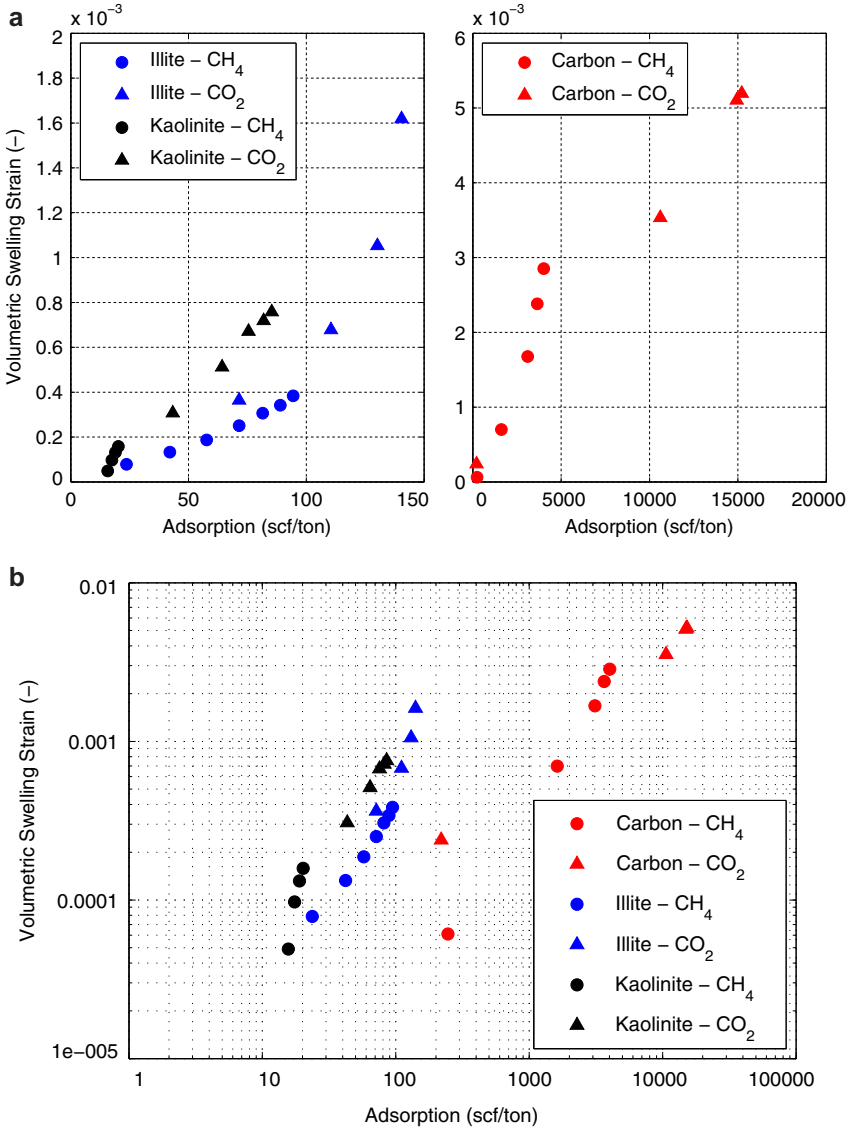

Fig. 8. (a) Linear scale: volumetric swelling strain as a function of the amount of adsorbed methane (circles) and carbon dioxide (triangles). The data suggests an approximately linear relationship between the observed swelling strain and the amount of adsorption. Moreover, for a given amount of adsorption, the stiffer the mineral, the less the amount of observed swelling strain. (b) Log–log scale: volumetric swelling volumetric swelling strain as a function of the amount of adsorbed methane (circles) and carbon dioxide (triangles). Scaled accordingly, all data is able to fit on the same graph, and the relative magnitude of adsorption and swelling by the carbon sample is more easily compared to the clay.

1000 psi lies within the same range as both of these studies. We are not aware of any adsorption isotherms for Montney, Marcellus or Eagle Ford shale samples within the literature at the time of this writing.

To date there have only been two published papers on CO_2 adsorption in gas shales. Nuttall et al. (2005) measured CH_4 and CO_2 adsorption on Devonian black-shale samples from Kentucky. They found Langmuir-like CO_2 adsorption that was approximately 5 times greater than the amount of CH_4 adsorption. In the same study as their CH_4 measurements, Kang et al. (2010) measured CO_2 adsorption on the same two Barnett shale samples. Their measurements were taken at CO_2 pressures from 2000 to 4000 psi, which is higher than the pressure range over which our measurements were taken (50–800 psi). Moreover, their measurements

were made at an unspecified temperature. Nevertheless, they extrapolate their isotherms to a CO_2 adsorption capacity of ~140 scf/ton at 500 psi in one sample, and ~250 scf/ton at 500 psi in the other. This is approximately 5 times and 10 times greater than the CH_4 adsorption they measured in the two samples at that pressure, respectively. The CO_2 adsorption capacity of our Barnett sample was about 75 scf/ton at 500 psi, which is about 2× the amount of methane adsorption measured at that pressure.

All experimental data was corrected for the volume of the adsorbed phase as previously described. An example of the data both before and after the correction is shown in Fig. 9 for the Barnett shale sample. For this particular sample, failing to account for the volume occupied by the adsorbed phase results in underestimating the quantity of adsorbed gas and total gas storage by about 10%.

Of particular interest is the question of how important the adsorbed phase is in terms of producible gas in place. In Fig. 10, we show production of free, adsorbed and total methane as a function of pressure for the four shale samples tested in this study. All estimates were made at 40 °C (experimental conditions) and assuming equal porosity (8%) and water saturation (25% of the pore volume occupied by water) for the sake of comparison. These assumptions result in an equivalent free gas production from all samples, allowing us to focus on the impact of the different adsorption isotherms between samples. By looking at the height of the total gas production at zero pressure, we see that the higher the adsorptive capacity (higher the Langmuir volume) the greater the quantity of adsorbed (and therefore total) gas produced. The most important observation made clear by the figure is that, for rocks in which these isotherms are representative, adsorption would be relatively unimportant in terms of producible gas in place. However, we are careful not to generalize this result, and acknowledge the high degree of heterogeneity that exists between different formations, and even between different lithologies within the same formation.

Our results also suggest the importance of isotherm shape, which is evident by comparing the Barnett and Montney samples. Despite having a higher capacity for adsorption (higher Langmuir volume), close inspection of the isotherm at 1000 psi shows us that the Montney sample would have produced slightly more adsorbed (and therefore total) gas per ton of rock. The adsorption isotherm for the Montney has a relatively high Langmuir pressure, allowing for greater desorption at higher pressures. Given that a large portion of the reservoir may never experience pressures lower than 1000 psi, it may be fair to say that isotherm shape is as important as total adsorption capacity when answering the question of how important adsorbed gas will be to overall production.

Our adsorption measurements on clay minerals showed a much larger than expected amount of adsorption if one were to assume the total adsorptive capacity of a rock to be roughly equal to the sum of the capacities of its mineral constituents. Similar results have been found by other authors, as described in the introduction (Schettler et al., 1991; Lu et al., 1995; Ross and Bustin, 2009). One potentially important factor is compaction and the microstructural difference between the ground clay minerals used in our experiments and their in-situ structure. Another important factor is likely water. We suspect that water adsorption plays an important role in regulating the amount of free surface area available for other molecules to adsorb. Passey et al. (2010) reported that much of the water present in shale gas systems is likely adsorbed on and associated with the surface of clay minerals. Recall that in preparing our shale and clay samples for adsorption, they were dried in a vacuum oven for an extended period of time. Thus, clay surfaces that would be largely occupied by water in situ were likely available for adsorption during our experiments. This would impact both our pure clay and shale adsorption measurements, resulting in an overestimation of methane (and carbon dioxide) adsorption in both cases. Water adsorption and the impact it might have on CH_4 and CO_2 adsorption remains a major experimental challenge to be overcome.

Another potential factor impacting our adsorption measurements on clay minerals is the difference between.

Swelling

Another challenging issue is the relationship between stress, strain and adsorption/desorption. We have successfully measured the volumetric swelling strain associated with the adsorption of CH_4 and CO_2 on carbon and clay samples to be on the order of 10^{-5} to 10^{-3}. In order to establish that swelling from adsorption is the cause of the observed volumetric strain, the swelling response to helium as a pore fluid was measured as well. Helium is an inert gas, and therefore non-adsorbing. An example of volumetric strain versus pressure is shown in Fig. 11, demonstrating that swelling strain is not observed in the case of helium.

Rather than examine adsorption as a function of pressure, it is more useful to evaluate swelling as a function of the amount of

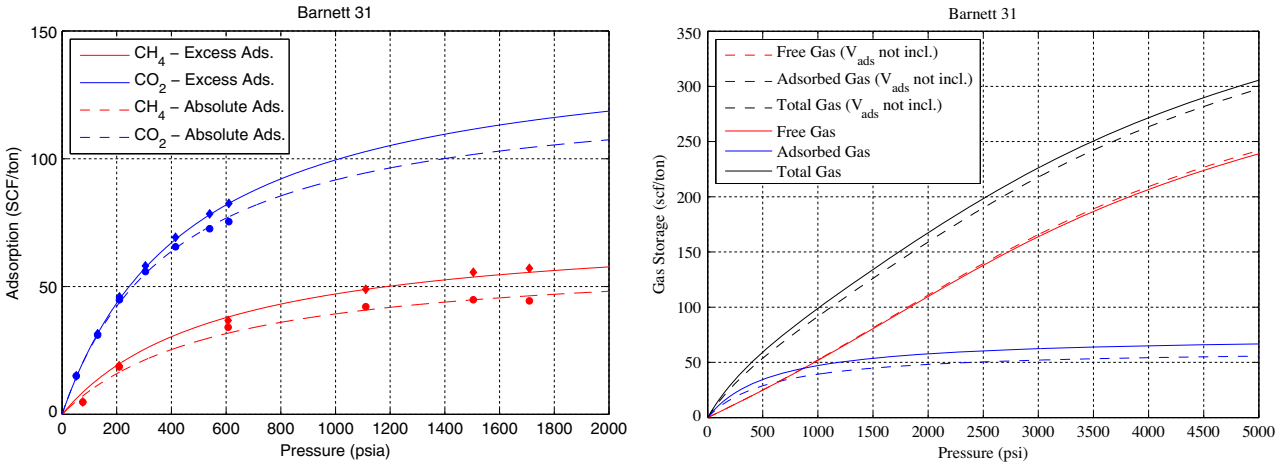

Fig. 9. Left: Barnett excess and total adsorption. Total adsorption calculation required correcting for the volume occupied by the adsorbed phase, as described in the methodology section. Right: Free CH_4, adsorbed CH_4 and total CH_4 storage of the Barnett sample as a function of pressure. Solid lines indicated data that has been corrected for the volume of the adsorbed phase, while dashed lines indicate the same data without the correction. If the correction is not made, both the adsorbed and total storage capacity of the rock is underestimated, and the free gas capacity is slightly overestimated due to the pore volume occupied by the adsorbed phase.

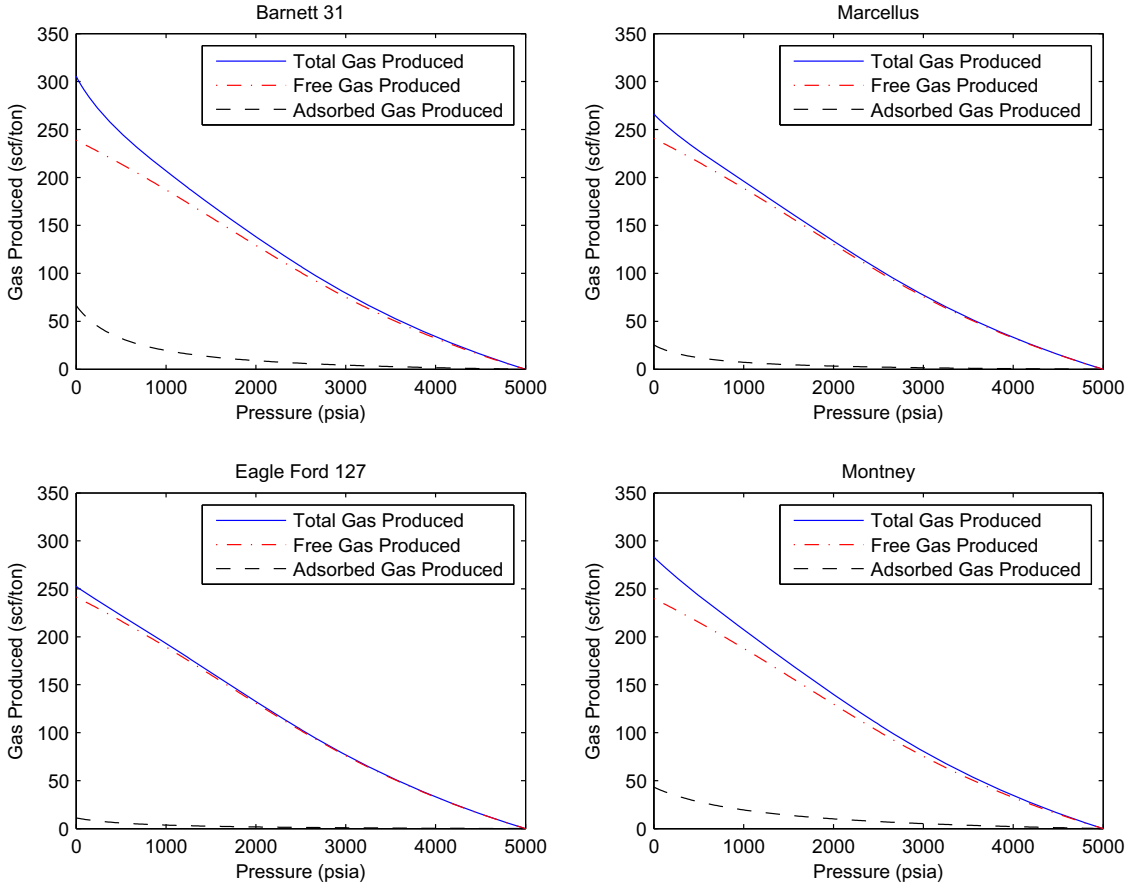

Fig. 10. Production of free, adsorbed and total methane as a function of pressure. All estimates were made at 40 °C and assuming equal porosity and water saturation for ease of comparison.

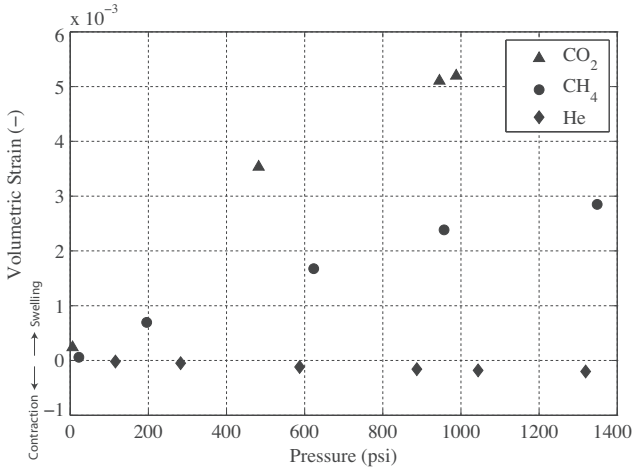

Fig. 11. An example of volumetric strain versus pressure for the activated carbon sample. Note that no swelling is observed when helium is the pore fluid, as helium is an inert (and therefore non-adsorbing) gas.

adsorption. The magnitude of the swelling strain is clearly dependent on the quantity of adsorption, as shown in Fig. 8. Moreover, there seems to be a material dependence. For a given amount of adsorption, the magnitude of the associated strain varies by approximately one order of magnitude. We hypothesize that this variance might be attributed to a difference in mineral stiffness.

It is difficult to speculate on the implications of the swelling strains we have measured. The strains we report are observed at the bulk/sample scale, and how this translates to strain at the pore scale, where adsorption and transport are occurring, is unknown. Kowalczyk et al. (2010) modeled adsorption-induced deformation on microporous carbons and made several interesting observations. They calculated the stresses resulting from adsorption/condensation in micropores to be on the order of 1000 GPa, and predicted strains at the bulk scale on the order of 10^{-3} caused entirely by deformation at the micropore scale. Future studies might focus on developing fully coupled simulations of adsorption, deformation and transport at this scale to better understand how this might impact production in shales.

Conclusions

We measured the adsorptive capacity of four gas shale samples as well as samples of pure carbon, illite and kaolinite. The Barnett shale sample had the highest TOC and adsorbed the most, followed by the Montney, Marcellus and Eagle Ford sample. The carbon sample adsorbed an extremely large amount, however, the extent to which it can be thought of as an analog to the organic content of shales is unknown. Illite and kaolinite also exhibited a relatively high capacity for adsorption. Similar to other studies, we find difficulty in describing shale adsorption isotherms as being the sum of the isotherms of its mineral constituents.

From an enhanced recovery or the CO_2 storage perspective, our results are quite favorable. We have shown that CO_2 has a higher capacity for adsorption in four different shale samples as well as

the major mineral constituents shale is comprised of. Follow up studies might investigate the preferential adsorption of CO_2 in a mixed gas setting.

It has been suggested that the desorption of methane might be partially responsible for the relatively long and flat production tails that have been observed in some shale reservoirs (Valko and Lee, 2010). The results presented in this paper demonstrate the increased importance of adsorption to production as pressure decreases. However, the magnitude of adsorption in the four shale samples examined in this paper was relatively small, and for these rocks, the adsorbed phase would be relatively unimportant in terms of producible gas in place. Other formations, or even other lithologies within the same formations, may yield entirely different results. Moreover, comparing adsorption isotherms for the Barnett and Montney samples underscores the importance of considering not just the adsorption capacity of the rock, but the shape of the adsorption isotherm as well.

Finally, we demonstrated the swelling nature of carbon and clay minerals in response to adsorption. Future experiments and simulations are required to better understand the relationship between adsorption, swelling and transport in gas shales, and how adsorption-induced deformation might impact production.

Acknowledgements

We gratefully acknowledge financial support from the Department of Energy (Grant DE-FE-0004731), BP, the Research Partnership to Secure Energy for America (RPSEA), and the Stanford Rock and Borehole Geophysics consortium (SRB). In addition, we would like to thank ConocoPhillips and BP for providing samples for us to work with.

References

Bustin, R.M., Bustin, A.M.M., Cui, A., Ross, D., Pathi, V.M., 2008, Impact of shale properties on pore Structure and storage characteristics: SPE Shale Gas Production Conference.

Chalmers, G.R., Bustin, R.M., 2008. Lower Cretaceous gas shales in northeastern British Columbia, Part I: geological controls on methane sorption capacity. Bull. Can. Pet. Geol. 56 (1), 1–21.

Cui, X., Bustin, A.M.M., Bustin, R.M., 2009. Measurements of gas permeability and diffusivity of tight reservoir rocks: different approaches and their applications. Geofluids 9, 208–223.

Dubinin, M.M., 1960. The potential theory of adsorption of gases and vapors for adsorbents with energetically nonuniform surfaces. Chem. Rev. 60 (2), 235–241.

Heller, R., Vermylen, J., Zoback, M., 2014. Experimental investigation of matrix permeability of gas shales. AAPG Bull. 98 (5), 975–995.

Hol, Sander., Peach, Colin J., Spiers, Christopher J., 2011. Applied stress reduces the CO_2 sorption capacity of coal. Int. J. Coal Geol. 85 (1), 128–142.

Kang, S.M., Fathi, E., Ambrose, R.J., Akkutlu, I.Y., Sigal, R.F., 2010. Carbon dioxide storage capacity of organic-rich shales. SPE 134583, 1–17.

Kowalczyk, P., Furmaniak, S., Gauden, P.A., Terzyk, A.P., 2010. Carbon dioxide adsorption-induced deformation of microporous carbons. J. Phys. Chem. C 114, 5126–5133.

Langmuir, I., 1916. The constitution and fundamental properties of solids and liquids: Part I, Solids. J. Am. Chem. Soc. 38 (11), 2221–2295.

Lin, W., Tang, G.Q., Kovscek, A.R., 2007. Sorption-induced permeability change of coal during gas-injection processes. In: SPE Annual Technical Conference and Exhibition. Society of Petroleum Engineers.

Loucks, R.G., Reed, R.M., Ruppel, S.C., Jarvie, D.M., 2009. Morphology, genesis, and distribution of nanometer-scale pores in siliceous mudstones of the Mississippian Barnett Shale. J. Sediment. Res. 79 (12), 848–861.

Lu, X.C., Li, F.C., Watson, A.T., 1995. Adsorption measurements in Devonian shales. Fuel 74 (4), 599–603.

Menon, P.G., 1968. Adsorption at high pressures. Chem. Rev. 68 (3), 277–294.

Montgomery, S.L., Jarvie, D.M., Bowker, K.A., Pollastro, R.M., 2005. Mississippian Barnett Shale, Fort Worth basin, north-central Texas: Gas-shale play with multi–trillion cubic foot potential. AAPG Bull. 89 (2), 155–175.

NIST, 2007, NIST Reference Fluid Thermodynamic and Transport Properties Database (REFPROP): Version 9.0.

Nuttall, B. C., Eble, C. F., Drahovzal, J. A., Bustin, R. M., 2005. Analysis of Devonian black shales in Kentucky for potential carbon dioxide sequestration and enhanced natural gas production. Report Kentucky Geological Survey/ University of Kentucky (DE-FC26-02NT41442).

Passey, Q., Bohacs, K., Esch, W., Klimentidis, R., Sinha, S. (2010, June). From oil-prone source rock to gas-producing shale reservoir-geologic and petrophysical characterization of unconventional shale gas reservoirs. In International Oil and Gas Conference and Exhibition in China.

Peters, K.E., Moldowan, J.M., 1993. The Biomarker Guide: Interpreting Molecular Fossils in Petroleum and Ancient Sediments, vol. 363. Prentice Hall, Englewood Cliffs, NJ.

Ross, Daniel J.K., Marc Bustin, R., 2007. Impact of mass balance calculations on adsorption capacities in microporous shale gas reservoirs. Fuel 86 (17), 2696–2706.

Ross, D.J., Marc Bustin, R., 2009. The importance of shale composition and pore structure upon gas storage potential of shale gas reservoirs. Mar. Pet. Geol. 26 (6), 916–927.

Schettler, P. D., Parmely, C. R., & Juniata, C. (1991). Contributions to total storage capacity in Devonian shales. SPE paper, 23422.

Sondergeld, C.H., Ambrose, R.J., Rai, C.S., Moncrieff, J., 2010, Micro-structural studies of gas shales: SPE Unconventional Gas Conference.

Tsai, M.C. et al., 1985. Adsorption of gas mixture on activated carbon. Carbon 23 (2), 167–173.

Valko, P., Lee, W. (2010, September). A better way to forecast production from unconventional gas wells. In SPE Annual Technical Conference and Exhibition.

Wang, F.P., Reed, R.M., 2009, Pore networks and fluid flow in gas shales: SPE Annual Technical Conference and Exhibition.